Published in final edited form as:
Adv Healthc Mater. 2015 February ; 4(3): 367–376. doi:10.1002/adhm.201400336.

Monocyte-Targeting Supramolecular Micellar Assemblies: A Molecular Diagnostic Tool for Atherosclerosis

Dr. E. J. Chung, **K. Nord**, **M. J. Sugimoto**[+], **E. Wonder**[++], and **Prof. M. Tirrell***
Institute for Molecular Engineering, University of Chicago, 5747 S. Ellis Ave., Chicago, IL 60637, USA

L. B. Mlinar
Institute for Molecular Engineering, University of Chicago, 5747 S. Ellis Ave., Chicago, IL 60637, USA

Department of Chemical and Biomolecular Engineering, University of California, Berkeley, 201 Gilman Hall, Berkeley, CA 94720, USA

Prof. F. J. Alenghat
Section of Cardiology, Department of Medicine, University of Chicago, 5841 S. Maryland Ave., Chicago, IL 60637, USA

Prof. Y. Fang
Section of Pulmonary and Critical Care, Department of Medicine, University of Chicago, 5841 S. Maryland Ave., Chicago, IL 60637, USA

Abstract

Atherosclerosis is a multifactorial inflammatory disease that can progress silently for decades and result in myocardial infarction, stroke, and death. Diagnostic imaging technologies have made great strides to define the degree of atherosclerotic plaque burden through the severity of arterial stenosis. However, current technologies cannot differentiate more lethal “vulnerable plaques,” and are not sensitive enough for preventive medicine. Imaging early molecular markers and quantifying the extent of disease progression continues to be a major challenge in the field. To this end, monocyte-targeting, peptide amphiphile micelles (PAMs) are engineered through the incorporation of the chemokine receptor CCR2-binding motif of monocyte chemoattractant protein-1 (MCP-1) and MCP-1 PAMs are evaluated preclinically as diagnostic tools for atherosclerosis. Monocyte-targeting is desirable as the influx of monocytes is a marker of early lesions, accumulation of monocytes is linked to atherosclerosis progression, and rupture-prone plaques have higher numbers of monocytes. MCP-1 PAMs bind to monocytes in vitro, and MCP-1 PAMs detect and discriminate between early- and late-stage atherosclerotic aortas. Moreover,

mtirrell@uchicago.edu.
[+]Present address: Department of Medicine, Creighton University, 2500 California Plaza, Omaha, NE, 68178, USA
[++]Present address: Department of Materials, University of California, Santa Barbara, MRL Building, Santa Barbara, CA, 93106, USA.

Supporting Information
Supporting Information is available from the Wiley Online Library or from the author.

There are no conflicts of interests.

MCP-1 PAMs are found to be eliminated via renal clearance and the mononuclear phagocyte system (MPS) without adverse side effects. Thus, MCP-1 PAMs are a promising new class of diagnostic agents capable of monitoring the progression of atherosclerosis.

1. Introduction

Atherosclerotic cardiovascular disease affects approximately 84 million American adults, leads to myocardial infarction and cerebral accidents, and accounts for more deaths than any other disease both in the US and worldwide.[1] Atherosclerosis is an inflammatory disease characterized by heightened immunological activity and the build-up of lipid-rich plaques. The progression of atherosclerotic plaques is initiated by the accumulation of cholesterol particles within the artery wall. Subsequently, endothelial cells lining the wall undergo activation, which includes the secretion of monocyte chemoattractant protein-1 (MCP-1, also known as C–C chemokine ligand 2), a chemokine which binds to the C–C chemokine receptor, CCR2, found on the monocyte surface, recruiting them in large quantities.[2,3] Monocytes differentiate into macrophages, ingesting and overloading on lipid particles, and thereby transform into foam cells. This results in amplification of the local inflammatory response, leads to further tissue injury through the secretion of more cytokines, chemokines, and toxic oxygen and nitrogen radicals, and precedes the formation of mature plaques, or atheromas, consisting of a lipid-rich, necrotic core surrounded by a fibrous cap.[4]

Monocyte accumulation in the arterial wall is observed in fatty streaks, the earliest visible lesion of human and experimental atherosclerosis. In the ApoE knock-out mouse, the most commonly used and well-characterized animal model of atherosclerosis, monocyte accumulation is continuous and proportional to disease progression.[5] Furthermore, in the absence of monocyte migration, atherosclerosis development is greatly hindered.[6] In humans, the dynamics of accumulation is not as well understood, although rupture-prone plaques in patients also contain higher numbers of monocytes.[7]

Targeting monocytes as a strategy to diagnose atherosclerosis could yield a molecular imaging tool that would detect the early onset of atherosclerosis, quantify the extent of plaque progression, and identify plaques most vulnerable to precipitous rupture and subsequent myocardial infarctions or strokes. Today, the main imaging technologies for atherosclerosis include intravascular ultrasound (IVUS), computed tomography (CT), positron emission tomography (PET), nuclear perfusion imaging, and magnetic resonance imaging (MRI). Although these imaging techniques have made great strides to assess the state of atherosclerotic plaques, poor sensitivity, limited accuracy and reproducibility, safety concerns, cost efficiency, and the subjective interpretation of results has hindered their use.[8,9] Perhaps the biggest drawback of these technologies is the difficulty in correlating physical traits such as fibrous cap thickness or % area of the necrotic core to the molecular state of a plaque.

While atherosclerosis is one of the leading causes of morbidity and mortality worldwide, atherosclerosis is underserved by the nanomaterials community.[10] In order to image atherosclerotic plaques effectively through the use of a molecular target, we have previously developed a clot-binding peptide amphiphile micelle (PAM).[11] Peptide amphiphiles (PAs)

are a class of synthetic molecules in which a biologically active peptide “headgroup” is chemically linked to a hydrophobic “tail.”[12-14] Under aqueous conditions, the PAs self-assemble into micelles in which the tails form the core, sequestered from water, and the peptides are displayed on the exterior as part of the corona. PAMs are advantageous because the corona provides a locally concentrated multivalent peptide display, which can potentiate binding to a target of interest.[14,15] Furthermore, the nanometer size provides favorable pharmacokinetic properties as well as permeability into leaky vasculature that exists in developing disease pathologies in vivo.[16,17] Moreover, monocytes enter plaques from the luminal side of the arterial wall, allowing for accessibility to intravenously delivered particles. In previous work, when the fibrin-targeting peptide, cysteine-arginine-glutamic acid-lysine-alanine (CREKA, previously identified via in vivo phage display), was used as the headgroup, these PAMs localized to microthrombi residing within the shoulder portion of atherosclerotic plaques, a location most prone to rupture, within the well-known murine ApoE knock-out model of atherosclerosis.[11] While visualization of fibrin within plaques is a powerful diagnostic tool, the presence of clots represents a very advanced stage of atherosclerosis, limiting the nanoparticle system to detecting high-risk, far downstream developments of plaque instability and providing only a narrow window of opportunity for disease management for the patient.[18,19]

In order to address the challenge of enabling earlier detection of atherosclerotic plaques and intervene during the evolving pathology of plaque formation and vulnerability, we elected to engineer spherical, monocyte-targeting PAMs through the incorporation of the CCR2-binding motif of MCP-1 in this study. We tested the ability of MCP-1 PAMs to bind to monocytes in vitro, and evaluated their ability to target and differentiate between varying stages of atherosclerosis in the ApoE knock-out mouse after 24 h. Moreover, we evaluate the initial clearance and biodistribution properties, as well as toxicity of these novel PAMs.

2. Results

2.1. Design and Characterization of MCP-1 PAMs

To construct monocyte-targeting PAMs, the CCR2-binding motif (residues 13–35) of MCP-1, YNFTNRKISVQRLASYRRITSSK, was modified by adding a cysteine residue to the N-terminus and was conjugated via a thioether linkage to 1,2-distearoyl-sn-glycero-3-phosphoethanolamine-*N*-[amino(polyethylene glycol)-2000] DSPE-PEG(2000)-maleimide (**Figure 1**A, Figure S1, Supporting Information). Control, non-targeting PAMs were constructed by conjugating a scrambled sequence of the MCP-1 peptide to the hydrophobic tail. The physicochemical properties of the hydrophobic tails and the interactions between peptide headgroups specify the supramolecular geometry, and the interposition of PEG between cell-specific, targeting peptides and a distearoyl lipid tail favors formation of uniform, small spherical micelles optimal for intravascular injection.[11,20] Furthermore, the incorporation of PEG enhances the clearance properties and lifetime of the micelles.[21] Fluorescently labeled micelles were constructed for imaging by mixing DSPE-PEG(2000)-Cy7 with either DSPE-PEG(2000)-MCP-1 or DSPE-PEG(2000)-scrambled in a 10:90 molar ratio. Cy7 was chosen as the fluorophore to be incorporated into micelles because its excitation and emission wavelengths in the near-infrared range are optimal to achieve both

deep tissue penetration and low auto-fluorescence for in vivo imaging, and 10 mol% Cy7 maximizes the fluorescence signal without quenching (Figure S2, Supporting Information).[22]

The critical micelle concentrations (CMCs) of resulting MCP-1 and scrambled PAMs were determined to be 2.2×10^{-6} and 1.6×10^{-6} M, respectively, via the 1,6-diphenyl-1,3,5-hexatriene (DPH) fluorescence assay[23] (**Table 1**), which are comparable to micellar systems composed of DSPE-PEG(2000). Transmission electron microscopy (TEM) and dynamic light scattering (DLS) confirmed the presence of spherical micelles with an average diameter of 14.7 ± 1.4 and 13.1 ± 1.4 nm (Figure 1B and Table 1).[20] Zeta potential measurements indicated that both MCP-1 and scrambled PAMs were positively charged (11.6 ± 0.1 and 10.9 ± 3.4 mV, respectively, Table 1); however, circular dichroism (CD) showed that the two peptides differed in secondary structure. The secondary structure of the free MCP-1 peptide sequences consisted of 34.2 ± 3.5% beta sheet, 65.8 ± 3.5% random coil, and 0.0 ± 0.0% alpha helix, while scrambled peptides consisted of 37.5 ± 6.2% beta sheet, 62.5 ± 6.2% random coil, and 0.0 ± 0.0% alpha helix (Table 1). Upon micellization, the secondary structure was enhanced (MCP-1 PAMs: 45.9 ± 1.0% beta sheet, 53.4 ± 1.6% random coil, and 0.7 ± 0.7% alpha helix; scrambled PAMs consisted of 60.9 ± 2.9% beta sheet, 38.8 ± 2.3% random coil, and 0.3 ± 0.7% alpha helix, Table 1). The PEG spacer drives spherical micelle formation by swelling the corona, but does not promote peptide folding as strongly as tighter tethering does. Both peptide sequence and secondary structure contribute to the specific recognition of MCP-1 PAMs by the CCR2 receptor and the mode of interaction with the cell membrane.[14,24] It may be possible to enhance this interaction further by further stabilization of a specific secondary structure, which we will examine in future work.

2.2. MCP-1 PAMs Bind to Monocytes and are Biocompatible In Vitro

To verify the specificity of Cy7-MCP-1 PAM binding with monocytes, the murine monocyte cell line WEHI-274.1 was used in vitro. Confocal fluorescence microscopy showed specific binding of monocytes to Cy7-MCP-1 PAMs after 1 h, with little to no binding with the Cy7-scrambled PAM control (**Figure 2**A). Inhibition of nonspecific uptake by phagocytic monocytes after 1 h may be attributable to PEG, which has been previously shown to shield particles from phagocytosis in the absence of a targeting peptide.[25] To test the eventual applicability for in vivo applications, biocompatibility of both MCP-1 and scrambled PAMs with WEHI-274.1 and primary murine aortic endothelial cells (mAECs) after a 24 h incubation was confirmed using the Live/Dead cell viability assay (Figure 2B). Over 99% of both cell types were viable upon treatment with either micelle and were comparable to phosphate buffer saline (PBS)-treated samples (Figure S3, Supporting Information).

2.3. Detecting and Discriminating Various Stages of Atherosclerosis

Following in vitro studies, we investigated targeting of Cy7-MCP-1 PAMs to monocytes in vivo and determined the potential for Cy7-MCP-1 PAMs as a platform for atherosclerosis diagnostics upon intravenous administration in the murine ApoE knock-out model. As monocyte accumulation increases with disease progression in this model, we hypothesized

that the amount of Cy7-MCP-1 PAM binding and the corresponding fluorescence signal in the early and late stages of the disease would reflect this phenomenon.[5] The concentration and volume of micelles utilized for in vivo studies were such that it remained above the CMC even upon injection in the total blood volume in circulation.[11,26] Ex vivo imaging after 24 h in circulation confirmed the specificity of Cy7-MCP-1 PAMs to the aorta in comparison to control, Cy7-scrambled PAMs (**Figure 3**). Quantitative comparisons supported the specificity of Cy7-MCP-1 PAMs binding to aortas in both stages of atherosclerosis, as compared to Cy7-scrambled PAMs. Furthermore, the level of Cy7-MCP-1 PAM binding to aortas of advanced stages of the disease ($5.3 \times 10^7 \pm 9.9 \times 10^6$ radiance (p/s/cm^2/sr)) was significantly higher than in the early stage ($2.7 \times 10^7 \pm 5.7 \times 10^6$ radiance (p/s/cm^2/sr), $p \leq 0.05$, Figure 3B). Approximately 0.06% and 0.16% of total MCP-1 PAMs injected accumulated within early- and late-stage atherosclerotic aortas, respectively.

Histological examination of the aortic arch revealed Cy7-MCP-1 PAMs accumulated primarily on the luminal surface of the vessel wall in mice with early stage atherosclerosis and on plaques in mice with late stage atherosclerosis, which overlapped with CCR2 expression (Figure 3C). Mice treated with Cy7-scrambled PAMs displayed some background fluorescence, but the signal did not colocalize with monocytes, as confirmed via anti-CCR2 staining. This further substantiated the binding capabilities of Cy7-MCP-1 PAMs to monocytes in vivo and demonstrated the ability of Cy7-MCP-1 PAMs to differentiate between the stages of atherosclerosis for diagnostic applications.

2.4. Clearance, Biodistribution, and Safety of MCP-1 PAMs

In vivo imaging confirmed Cy7-MCP-1 and Cy7-scrambled PAMs remained in the bloodstream after 24 h, indicated through a background level of fluorescence present throughout the body, which is consistent with our recent findings showing micelles are cleared from circulation after 7 d (**Figure 4**).[27] High accumulation of either PAM was detected in the bladder and liver, organs part of renal clearance and the monocyte phagocytic system (MPS, also called the reticuloendothelial system or RES), respectively. To further confirm partial elimination of micelles through renal clearance, urine was collected directly from the bladder and fluorescence measured (Figure 4B). An increase in Cy7 intensity was found for all samples when compared to PBS-injected samples (in arbitrary units, early MCP-1: 118.75 ± 11.40, early scrambled: 66.67 ± 14.43, late MCP-1: 88.89 ± 19.25, late scrambled: 85.42 ± 13.01, PBS: 44.80 ± 6.25).

Figure 4C shows the distribution of micelles within the heart, lung, liver, spleen, large intestines, kidney, and bladder and quantification is provided in Figure S4 (Supporting Information). Both types of PAMs were present in the bladder and the kidney as expected, as well as the liver and the spleen. However, histopathological evaluation of major organs did not detect abnormal lesions, and no apparent signs of tissue or cellular damage were observed in mice injected with Cy7-MCP-1 or Cy7-scrambled PAMs (**Figure 5**). Findings were comparable to organ structures obtained from mice injected with PBS.

In order to evaluate the potential cytotoxic effects of Cy7-MCP-1 or Cy7-scrambled PAMs on the two major organs of MPS, the liver and spleen, the activity of the apoptosis marker,

caspase-3, was measured (**Figure 6**). Caspase activity levels for all injected samples were comparable to that of PBS-treated animals. To assess liver function, liver tissue levels of alanine aminotransferase (ALT) and aspartate aminotransferase (AST) were measured (Figure 6C,D). For both biochemical parameters and all samples, no statistical differences were found in comparison to the PBS control, further confirming initial micelle biocompatibility and safety.

3. Discussion

Traditional imaging of atherosclerosis has focused on the % occlusion of the arterial lumen or the structure of plaque, and primarily provides anatomic and physiological information at relatively late stages of the disease.[28] Advances in the basic and clinical biology of atherosclerosis have identified key inflammatory processes that contribute to lesion initiation, progression, and complication, and the emerging field of molecular imaging has harnessed this information to target specific biochemical markers for accurate, early diagnosis.[28,29] Nanosized micelles are suitable for molecular and cellular level imaging tools as they are small enough to interact with receptor targets with high specificity and avidity, owing to their multivalency, and provide high surface areas that can be decorated with targeting ligands and imaging agents to allow tracking of their distribution.[10] However, inspection and quantification of disease advancement have been particularly challenging due to the complex nature of atherosclerosis, which is characterized by multiple silent events that can evolve over decades, some fatal without warning. As a result, treatment or management, especially at early stages of the disease, proves difficult. In contrast, we show that MCP-1 PAMs bind to the CCR2 receptor and accumulate in the aortic arch in proportion to disease progression in the ApoE knockout mouse, offering a tool to both diagnose and differentiate between the stages of atherosclerosis, which can be expanded to assess other sites of plaque formation including the carotid, subclavian, and iliac arteries (Figure 3).[30] Consequently, MCP-1 PAM technology represents an important diagnostic paradigm for systemically targeting persistent markers of atherosclerosis that provide insight into the degree of vulnerability and therefore direct translation for specific and potentially personalized disease management regimens. It is important to note that although CCR2 is a well-known receptor on monocytes, activated endothelial cells have also been reported to express some CCR2 within plaques and may also be contributing to the targeting signal of MCP-1 PAMs in vivo.[31] Selectivity of MCP-1 PAMs for monocytes in vivo over other cell types encountered in the blood and vasculature will be further investigated in future studies.

Furthermore, the evaluation of tissue dissemination, clearance mechanisms, and toxicity is critical for preclinical assessment of diagnostic agents. Here, we show that PAMs are eliminated from the body via both renal clearance and MPS, causing no observable toxicity to organs involved 24 h post-circulation (Figure 4,5, and 6). Based on the 15 nm size of our micelles, our results are consistent with our recent findings and others who report nanoparticles >10 nm are cleared by the MPS, specifically through sequestration by sinusoids in the spleen and fenestra of the liver.[27] Particles <6 nm are distributed widely in a variety of organs by crossing tight endothelial junctions and are excreted through the renal system.[32] As our micelles are dynamic species, it is possible that upon reaching the

targeting site, only some amphiphile monomers bind, in turn causing micelle disassembly and clearance of non-bound monomers through the bladder. After 7 d, approximately 90% of micelles are cleared out of the body.[27]

In summary, we have combined a rational materials and biological approach to provide proof-of-concept that intravenously administered MCP-1 PAMs can target plaques and detect the extent of atherosclerosis in a mouse model. These nanoassemblies have the opportunity to advance atherosclerosis therapies by enhancing drug solubility through exploitation of the micelle's hydrophobic core, reducing the required dosage and potential for cytotoxicity via active targeting and focal delivery, increasing systemic circulation time of the carrier, and providing multifunctionality by combining therapeutic and diagnostic agents within one, theranostic system. Regarding additional imaging modalities, especially those that are clinically in use, modifications with radionuclides and contrast agents for PET and MRI such as copper 64 and gadolinium can be easily adapted into the modular design of micelles, providing enhanced spatial resolution with minimal interference from agents accumulated in other organs such as the liver.[33,34] Moreover, these imaging modalities adapted for micelles could then be combined with anti-inflammatory drugs for potential theranostic applications. In addition to micelles that target molecular or cellular markers, micelles can be further optimized to assess structural components of vulnerable plaques by imaging fibrous cap thickness and the area of the necrotic core via incorporation of collagen or metalloproteinase-binding peptides.[35] As monocytosis is characteristic to multiple inflammatory diseases, MCP-1 PAMs also have the potential to be employed in multiple applications.[36] Although the full extent of monocyte accumulation has not been fully tested in humans, PAMs may serve as a tool for discovery science as well, validating cellular abundance during the complex etiology of atherosclerosis.

4. Conclusion

We have designed and synthesized a novel, self-assembling PAM for targeting monocytes. These spherical micelles bind to monocytes in vitro and are effective at targeting atherosclerotic plaques in the ApoE knock-out mouse model after 24 h in circulation. Moreover, this system can quantitatively discriminate between early and late stages of atherosclerosis and does not cause adverse effects to vital organs. As the accumulation of monocytes is linked to atherosclerosis progression, MCP-1 PAMs are a promising tool for both diagnostic and preventive medicine, and have the potential to be developed as theranostic systems for a variety of diseases where inflammation is the underlying cause.

5. Experimental Section

Materials

Amino acids and solvents for peptide synthesis were purchased from Protein Technologies (Tucson, AZ). Wang resin was obtained from Anaspec (Fremont, CA). DSPE-PEG2000-maleimide and DSPE-PEG2000-amine were obtained from Avanti Polar Lipids (Alabaster, AL), Cyanine7 (Cy7) mono-N-hydroxysuccinimide ester from GE Healthcare Life Sciences (Pittsburgh, PA), and 400 mesh lacey carbon grids from Ted Pella (Redding, CA). mAECs, murine aortic smooth muscle cells (mASMCs), and M1168 or M2268 media were purchased

from Cell Biologics (Chicago, IL). Mouse monocytes, WEHI-274.1, were purchased from ATCC (Manassas, VA) and Dulbecco's modified Eagle's medium, fetal bovine serum, penicillin/streptomycin, and 2-mercaptoethanol from Sigma Aldrich (St. Louis, MO). The Live/ Dead assay kit was obtained from Molecular Probes (Eugene, OR). Mice with the *Apoe*^{tm1Unc} mutation (The Jackson Laboratory, Bar Harbor, ME) were fed a high-fat diet that consists of 21% (wt/wt) fat, 0.15% (wt/ wt) cholesterol, 19.5% (wt/wt) casein, and no sodium cholate (Harlan, Indianapolis, Indiana). The CCR2 primary antibody (ab32144) was purchased from Abcam (Cambridge, England). Biotinylated goat anti-rabbit IgG secondary antibody, Vectastain Elite ABC Kit, and Avidin/ Biotin Blocking Kit were obtained from Vector Laboratories (Burlingame, CA). OCT and DAB/DAB+ Chromogen Solution were purchased from Sakura Finetek (Torrance, CA) and DAKO (Darpinteria, CA), respectively. Fluorescence and colorimetric assay kits to measure ALT (MAK052), AST (MAK055), and caspase-3 activity (CASP3C) were derived from Sigma Aldrich (St. Louis, MO).

Micelle Synthesis

The CCR2-binding motif (residues 13–35) of the MCP-1 protein [YNFTNRKISVQRLASYRRITSSK] or scrambled peptide sequence [YNSLVFRIRNSTQRKYRASIST] was modified by adding a cysteine residue to the N-terminus for covalent conjugation to the micelle lipid tail. The MCP-1 peptide (0.25 mmol) was synthesized using standard Fmoc-mediated solid-phase peptide synthesis methods on a Wang resin using an automated PS3 Benchtop Peptide Synthesizer (Protein Technologies, Tucson, AZ). Peptides were cleaved/deprotected with 94:2.5:2.5:1 vol% TFA:1,2-ethanedithiol:H2O:triisopropylsilane (TIS) and were precipitated and washed several times with cold diethyl ether, dissolved in water, lyophilized, and stored as lyophilized powders at −20 °C. Crude peptide mixtures were purified by reverse-phase HPLC (Prominence, Shimadzu, Columbia, MD) on a C4 column (Waters, Milford, MA) at 55 °C using 0.1% trifluoroacetic acid in acetonitrile/ water mixtures and characterized by MALDI-TOF/TOF mass spectral analysis (Biflex III, Bruker, Billerica, MA). Cysteine-containing peptides (10–15 mg) were conjugated via a thioether linkage to DSPE-PEG2000-maleimide by adding a 10% molar excess of the lipid to peptide in water (2–3 mL). After reaction at room temperature for 24 h, the resulting product was purified and characterized as described above. The final concentration of PA in solution was determined using amino acid analysis (Molecular Structure Facility, UC Davis, Davis, CA). Cy7 (5 mg) was conjugated via an amide bond to DSPE-PEG2000-amine by adding an equal molar equivalent of Cy7 mono-N-hydroxysuccinimide ester to the lipid dissolved in 10×10^{-3} M aqueous sodium carbonate buffer (pH 8.5, 1–2 mL). After reaction at room temperature for 24 h, the mixture was also purified and characterized as described above. Fluorescently-labeled MCP-1 micelles were assembled by dissolving the Cy7 and peptide-containing DSPE-PEG(2000) amphiphiles in methanol, mixing the components, and evaporating the mixed solution under nitrogen. The resulting film was dried under vacuum overnight, and then hydrated at 80 °C for 30 min in water or PBS and allowed to cool to room temperature.

Transmission Electron Microscopy

Negative staining samples for TEM were prepared by placing the 100×10^{-6} M PAM solution on carbon grids for 2 min. Excess liquid was wicked away with filter paper and the

grid was washed with Milli-Q water before placing 1 wt% phosphotungstic acid solution for 2 min and washing with Milli-Q water. Dried samples were imaged on a JEOL 1230 TEM, immediately (JEOL, Ltd., Tokyo, Japan).

Dynamic Light Scattering

Stock solutions of 100×10^{-6} M PAM in PBS were used to confirm the presence of small spheroidal micelles and DLS measurements were determined at 90° and 637 nm using a Brookhaven Instruments system (Holtzville, NY) consisting of a BI-200SM goniometer and a BI-9000AT autocorrelator ($N \geq 3$ samples).

Zeta Potential

Zeta potential was determined by measuring 100×10^{-6} M DSPE-PEG(2000)-MCP-1 and DSPE-PEG(2000)-scrambled micelles dissolved in water (Zetasizer Nano ZS, Malvern, Worcestershire, United Kingdom, $N \geq 6$).

Circular Dichroism Spectroscopy

CD spectroscopy was performed on a Jasco J-815 spectropolarimeter (Easton, MD). Peptide and PA solutions (100×10^{-6} M) were analyzed using 0.2 mm path-length cuvettes at room temperature and measurements were collected at 0.5 nm intervals from 265 to 190 nm with a 1 s averaging time and a 1 nm bandwidth. Five scans were collected and the data were averaged. To quantify secondary structure, the CD spectra were fit by a linear combination of polylysine basis spectra.[37]

1,6-Diphenyl-1,3,5-hexatriene Fluorescence

The CMC was determined using DPH fluorescence.[23] This method relies on an increase in DPH fluorescence as it partitions from aqueous solution into the hydrophobic micelle core. Solutions of the MCP-1 and scrambled PA ranged in concentrations from 316×10^{-6} to 0.01×10^{-6} M. DPH was dissolved in tetrahydrofuran (THF) and a small amount of this solution was added to each PA solution to achieve 1×10^{-6} M DPH with a residual THF volume percentage of approximately 0.1. Solutions containing both PA and DPH were allowed to equilibrate for 1 h prior to measurement using a Tecan Infinite 200 plate reader (Männedorf, Switzerland). DPH was excited at 350 nm and fluorescence emission was measured at 428 nm.

Fluorescence Quenching of Micelles

To assess the optimal molar content of DSPE-PEG(2000)-Cy7 within a micelle, fluorescence signal quenching of 100×10^{-6} M micelle solutions consisting of varying molar % of DSPE-PEG(2000)-MCP-1 and DSPE-PEG(2000)-Cy7 were prepared in PBS and fluorescence signal measured (ex. 747 nm, em. 776 nm, HORIBA Scientific, FluoroMax-4, Edison, NJ).

Cell Culture

mAECs were cultured and expanded following the manufacturer's instructions. Mouse monocytes (WEHI-274.1) were cultured and expanded in Dulbecco's modified Eagle's

medium supplemented with 10% fetal bovine serum, 1% penicillin/streptomycin, and 0.05×10^{-3} M 2-mercaptoethanol. All cell types were cultured at 37 °C in a humidified incubator under 5% CO_2. Cells at passage five were used and media were changed every 2–3 d.

Micelle Binding In Vitro

Cell uptake of mixed micelles containing DSPE-PEG(2000)-Cy7:DSPE-PEG(2000)-MCP-1 and DSPE-PEG(2000)-Cy7:DSPE-PEG(2000)-scrambled (10:90 molar ratio) was examined using confocal microscopy. Monocytes (50 000) were cultured in glass bottom dishes and incubated with mixed micelles at a final concentration of 100×10^{-6} M suspended in full media for 1 h at 37 °C in a humidified incubator under 5% CO_2. Live imaging was conducted on a Fluoview FV1200 laser scanning confocal microscope (Olympus, Center Valley, PA, $N = 3$).

In Vitro Biocompatibility

To assess biocompatibility, 10 000 mAEC or 50 000 monocytes were cultured within 96-well plates and after 24 h, 20 μL of PBS or 1×10^{-3} M MCP-1 or scrambled PAMs were added to 180 μL of growth media (100×10^{-6} M final micelle concentration). After 24 h of incubation, cell viability was determined by a Live/Dead assay kit and imaged on a Leica DMI6000B fluorescence microscope (Buffalo Grove, IL, $N = 3$).

Targeting of MCP-1 PAMs to Atherosclerotic Plaques

In order to conduct proof-of-concept experiments to test the hypothesis that MCP-1 PAMs can target monocytes in atherosclerotic plaques as well as discriminate the extent of disease progression, female, four-week old, transgenic mice homozygous for the *Apoe*^{tm1Unc} mutation were fed a high-fat diet that consists of 21% (wt/wt) fat, 0.15% (wt/wt) cholesterol, 19.5% (wt/wt) casein, and no sodium cholate for 12 or 20–24 weeks to generate early-stage and late-stage lesions.[38,39] Mice were shaved and naired, and tail veins were dilated and sterilized with 70% ethanol before 100 μL of 1×10^{-3} M DSPE-PEG(2000)-Cy7:DSPE-PEG(2000)-MCP-1 or DSPE-PEG(2000)-Cy7:DSPE-PEG(2000)-scrambled (10:90 molar ratio) suspended in PBS were intravenously injected ($N \geq 3$). The control group consisted of mice with early-stage atherosclerosis treated with PBS alone, and all mice were chosen in random order and assigned randomly into each group by a third party. All mice were used for data collection. Micelles were allowed to circulate for 24 h before mice were anesthetized with 2.5% isoflurane in O_2 and whole body fluorescence imaging was conducted (IVIS 200, Xenogen, Caliper Life Sciences, Hopkinton, MA, USA). Mice were then euthanized via CO_2 overdose and the aorta, heart, lung, liver, spleen, large intestines, kidney, and bladder harvested. Near-infrared fluorescence imaging of organs was conducted using an IVIS 200 Imaging System (PerkinElmer, Downers Grove, IL). Urine samples were collected directly from the bladder, diluted 25x in PBS, and Cy7 intensity quantified on a 96-well plate (ex. 746 nm, em. 776 nm, Infinite 200 Pro, Tecan Group Ltd., Mannedorf, Switzerland) to assess clearance through the renal system. All animal procedures followed NIH guidelines for the care and use of laboratory animals and were approved by the University of Chicago's Institutional Animal Care and Use Committee (Chicago, IL).

Histology

Following optical imaging and euthanasia, the aorta, heart, lung, large intestines, liver, kidney, spleen, and bladder were fixed with 4% paraformaldehyde overnight at 4 °C. Tissue was then submerged in a 30% sucrose solution for 8 h and frozen in OCT before 5–7 μm samples were cryosectioned (Microm HM 525, Fisher Scientific, Pittsburgh, PA), stained with hemotoxylin and eosin (H and E), and imaged (DMI6000 B, Leica Microsystems, Inc., Buffalo Grove, IL). Unstained and DAPI-stained cross-sections of the aortic arch were imaged for micelles (Cy7) and cell nuclei, respectively, on a fluorescence microscope (DMI6000 B, Leica Microsystems, Inc., Buffalo Grove, IL). Representative images are presented.

Immunohistochemistry

Serial cross-sections (5–7 μm thick) of the aortic arch were mounted on silane-treated slides and allowed to air dry. Tissue sections were treated with 3% hydrogen peroxide, blocked with the Avidin/Biotin Blocking Kit, and 10% normal goat serum in TBS, and incubated with an antibody against CCR2 in a humidified chamber at room temperature for 1 h (1:150) to visualize monocytes. Slides were washed with TBS and incubated with biotinylated goat anti-rabbit IgG secondary antibody for 1 h and Vectastain Elite ABC Kit for 30 min at room temperature. Sections were developed using the DAB/DAB+ Chromogen Solution and counterstained with Gill III Hematoxylin. All sections were dehydrated, mounted, and evaluated using bright-field microscopy (DMI6000 B, Leica Microsystems, Inc., Buffalo Grove, IL). Representative images are presented.

Liver and Spleen Function

To assess liver function, an equal mass of tissue was homogenized in lysis buffer and liver levels of ALT and AST were measured using commercial assay kits. In addition, the level of apoptosis in the liver and spleen was determined by colorimetric quantification of caspase-3 activity.

Statistical Analysis

Data are expressed as mean ± SEM. A Student's *t*-test was used to compare means of pairs and analysis of variance (ANOVA) using Tukey multiple comparison test post-hoc analysis to determine significant differences among three or more means. A p value of 0.05 or less was considered to be significant.

Supplementary Material

Refer to Web version on PubMed Central for supplementary material.

Acknowledgements

This work was supported by the University of Chicago and the US Department of Energy Office of Science program in Basic Energy Sciences and the Materials Sciences and Engineering Division. The authors made use of the equipment and acknowledge assistance from the Mass Spectroscopy Facility, NSF Materials Research Science and Engineering Center (MRSEC), Integrated Microscopy Core Facility, Optical Imaging Core, and Human Tissue Resource Center at the University of Chicago. Funding: This work was supported by an American Heart

Association Postdoctoral Fellowship granted to E.J.C. and a DoD, AFOSR, National Defense Science and Engineering Graduate Fellowship, 32 CFR 168a to L.B.M.

References

[1]. Go AS, Mozaffarian D, Roger VL, Benjamin EJ, Berry JD, Borden WB, Bravata DM, Dai S, Ford ES, Fox CS, Franco S, Fullerton HJ, Gillespie C, Hailpern SM, Heit JA, Howard VJ, Huffman MD, Kissela BM, Kittner SJ, Lackland DT, Lichtman JH, Lisabeth LD, Magid D, Marcus GM, Marelli A, Matchar DB, McGuire DK, Mohler ER, Moy CS, Mussolino ME, Nichol G, Paynter NP, Schreiner PJ, Sorlie PD, Stein J, Turan TN, Virani SS, Wong ND, Woo D, Turner MB. Circulation. 2013; 127:e6. [PubMed: 23239837]

[2]. Szmitko PE, Wang C-H, Weisel RD, de Almeida JR, Anderson TJ, Verma S. Circulation. 2003; 108:1917. [PubMed: 14568885]

[3]. Libby P. Circulation. 2001; 104:1191.

[4]. Zhang X, Mosser DM. J. Pathol. 2008; 214:161. [PubMed: 18161744]

[5]. Swirski FK, Pittet MJ, Kircher MF, Aikawa E, Jaffer FA, Libby P, Weissleder R. Proc. Natl. Acad. Sci. 2006; 103:10340. [PubMed: 16801531]

[6]. Smith JD, Trogan E, Ginsberg M, Grigaux C, Tian J, Miyata M. Proc. Natl. Acad. Sci. 1995; 92:8264. [PubMed: 7667279]

[7]. Kashiwagi M, Imanishi T, Tsujioka H, Ikejima H, Kuroi A, Ozaki Y, Ishibashi K, Komukai K, Tanimoto T, Ino Y, Kitabata H, Hirata K, Akasaka T. Atherosclerosis. 2010; 212:171. [PubMed: 20684824]

[8]. ten Kate GL, Sijbrands EJ, Staub D, Coll B, ten Cate FJ, Feinstein SB, Schinkel AFL. Curr. Probl. Cardiol. 2010; 35:556. [PubMed: 20974314]

[9]. Low AF, Tearney GJ, Bouma BE, Jang I-K. Nat. Clin. Pract. Cardiovasc. Med. 2006; 3:154. [PubMed: 16505861]

[10]. Lewis DR, Kamisoglu K, York AW, Moghe PV. Wiley Interdiscip. Rev.: Nanomed. Nanobiotechnol. 2011; 3:400. [PubMed: 21523920]

[11]. Peters D, Kastantin M, Kotamraju VR, Karmali PP, Gujraty K, Tirrell M, Ruoslahti E. Proc. Natl. Acad. Sci. 2009; 106:9815. [PubMed: 19487682]

[12]. Hartgerink JD, Beniash E, Stupp SI. Proc. Natl. Acad. Sci. 2002; 99:5133. [PubMed: 11929981]

[13]. Missirlis D, Chworos A, Fu CJ, Khant HA, Krogstad DV, Tirrell M. Langmuir. 2011; 27:6163. [PubMed: 21488620]

[14]. Trent A, Marullo R, Lin B, Black M, Tirrell M. Soft Matter. 2011; 7:9572.

[15]. Hamley IW. Soft Matter. 2011; 7:4122.

[16]. Bisht S, Feldmann G, Koorstra J-BM, Mullendore M, Alvarez H, Karikari C, Rudek MA, Lee CK, Maitra A, Maitra A. Mol. Cancer Ther. 2008; 7:3878. [PubMed: 19074860]

[17]. Slevin M, Badimon L, Grau-Olivares M, Ramis M, Sendra J, Morrison M, Krupinski J. Mol. BioSyst. 2010; 6:444. [PubMed: 20174673]

[18]. Nighoghossian N, Derex L, Douek P. Stroke. 2005; 36:2764. [PubMed: 16282537]

[19]. Lobatto ME, Fuster V, Fayad ZA, Mulder WJM. Nat. Rev. Drug Discovery. 2011; 10:835.

[20]. Kastantin M, Ananthanarayanan B, Karmali P, Ruoslahti E, Tirrell M. Langmuir. 2009; 25:7279. [PubMed: 19358585]

[21]. Photos PJ, Bacakova L, Discher B, Bates FS, Discher DE. J. Controlled Release. 2003; 90:323.

[22]. Kobayashi H, Ogawa M, Alford R, Choyke PL, Urano Y. Chem. Rev. 2009; 110:2620. [PubMed: 20000749]

[23]. Chattopadhyay A, London E. Anal. Biochem. 1984; 139:408. [PubMed: 6476378]

[24]. Morris MC, Deshayes S, Heitz F, Divita G. Biol. Cell. 2008; 100:201. [PubMed: 18341479]

[25]. He Q, Zhang J, Shi J, Zhu Z, Zhang L, Bu W, Guo L, Chen Y. Biomaterials. 2010; 31:1085. [PubMed: 19880176]

[26]. Ashok B, Arleth L, Hjelm RP, Rubinstein I, Önyüksel H. J. Pharm. Sci. 2004; 93:2476. [PubMed: 15349957]

[27]. Chung EJ, Cheng Y, Morshed R, Nord K, Han Y, Wegscheid ML, Auffinger B, Wainwright DA, Lesniak MS, Tirrell MV. Biomaterials. 2014; 35:1249. [PubMed: 24211079]

[28]. Buxton DB, Antman M, Danthi N, Dilsizian V, Fayad ZA, Garcia MJ, Jaff MR, Klimas M, Libby P, Nahrendorf M, Sinusas AJ, Wickline SA, Wu JC, Bonow RO, Weissleder R. Circulation. 2011; 123:2157. [PubMed: 21576680]

[29]. Jaffer FA, Libby P, Weissleder R. J. Am. Coll. Cardiol. 2006; 47:1504.

[30]. Nakashima Y, Plump AS, Raines EW, Breslow JL, Ross R. Arterioscler. Thromb. 1994; 14:133. [PubMed: 8274468]

[31]. Weber KSC, Nelson PJ, Gröne H-J, Weber C. Arterioscler. Thromb. Vasc. Biol. 1999; 19:2085. [PubMed: 10479649]

[32]. Choi HS, Liu W, Misra P, Tanaka E, Zimmer JP, Ipe BI, Bawendi MG, Frangioni JV. Nat. Biotechnol. 2007; 25:1165. [PubMed: 17891134]

[33]. Lipinski MJ, Amirbekian V, Frias JC, Aguinaldo JGS, Mani V, Briley-Saebo KC, Fuster V, Fallon JT, Fisher EA, Fayad ZA. Magn. Reson. Med. 2006; 56:601. [PubMed: 16902977]

[34]. Xiao Y, Hong H, Javadi A, Engle JW, Xu W, Yang Y, Zhang Y, Barnhart TE, Cai W, Gong S. Biomaterials. 2012; 33:3071. [PubMed: 22281424]

[35]. Newby AC. Arterioscler. Thromb. Vasc. Biol. 2008; 28:2108. [PubMed: 18772495]

[36]. Yadav A, Saini V, Arora S. Clin. Chim. Acta. 2010; 411:1570. [PubMed: 20633546]

[37]. Greenfield NJ, Fasman GD. Biochemistry. 1969; 8:4108. [PubMed: 5346390]

[38]. Meir KS, Leitersdorf E. Arterioscler. Thromb. Vasc. Biol. 2004; 24:1006. [PubMed: 15087308]

[39]. Whitman SC. Clin. Biochem. Rev./Aust. Assoc. Clin. Biochem. 2004; 25:81.

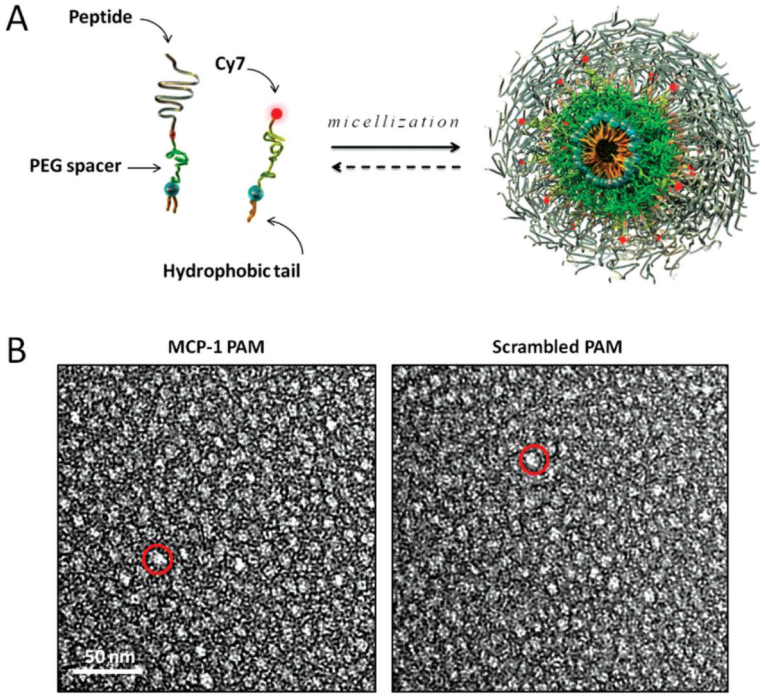

Figure 1.

Design and structure of MCP-1 PAMs. A) Schematic depicting PAM self-assembly. PAs consist of a distearoyl hydrophobic tail (two 18-carbon chains) and a PEG spacer that was conjugated to the MCP-1 peptide that corresponds to the CCR2-binding motif (residues 13–35), scrambled peptide, or the Cy7 fluorophore. Fluorescently-labeled, mixed micelles consisted of peptide-containing and Cy7-labeled amphiphiles in a 90:10 molar ratio. B) Representative TEM images of MCP-1 PAMs (L) and scrambled PAMs (R). Both micelles are spherical in shape with a diameter on the order of 10 nm.

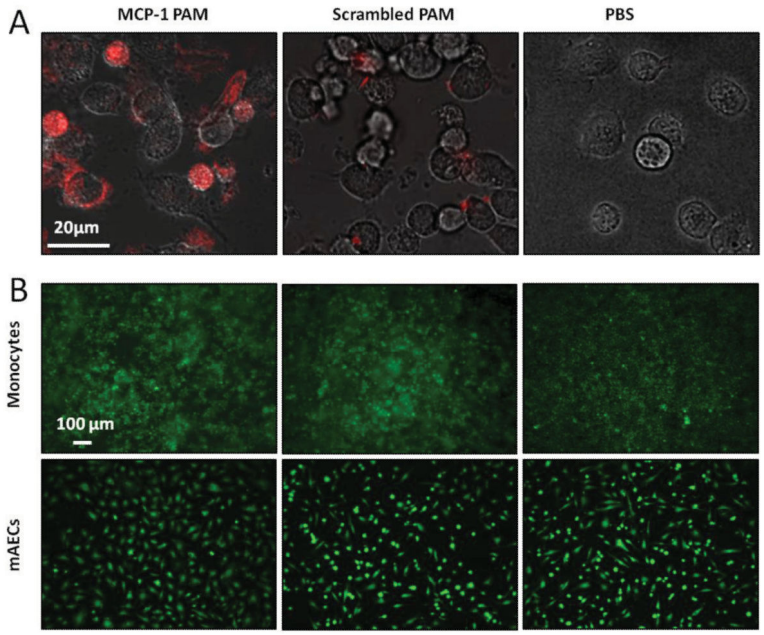

Figure 2.

MCP-1 PAMs bind to monocytes and are biocompatible in vitro. A) Confocal fluorescence microscopy of Cy7-MCP-1 PAMs binding to the murine monocytic cell line, WEHI-274.1, after 1 h. B) Biocompatibility of MCP-1 and scrambled PAMs with WEHI-274.1 and primary murine aortic endothelial cells (mAECs) after 24 h was determined in vitro using the Live/Dead cell viability assay and were comparable to PBS-treated samples (live cells: green).

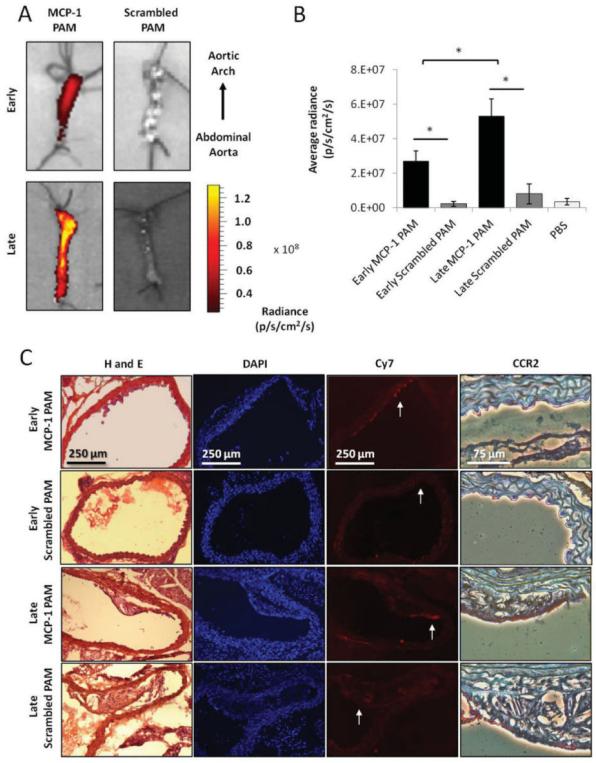

Figure 3.

MCP-1 PAMs detect and discriminate between stages of atherosclerosis in vivo**.** Optical imaging of early- and late-stage atherosclerotic aortas of ApoE knock-out mice injected with A) MCP-1 PAMs or scrambled PAMs after 24 h. Representative aortas are shown. B) Quantification of micelle binding. Data points are mean ± SD, $*P < 0.05$, $N \geq 3$ mice. C) Representative histological and immunohistochemical staining of cross-sections derived from early- and late-stage atherosclerotic aortas treated with MCP-1 or scrambled PAMs. From left to right: H and E, DAPI, Cy7 (PAM) signal, and magnified regions showing CCR2 expression via DAB staining (brown). Arrows in the Cy7 images denote the region that was magnified in corresponding CCR2 image.

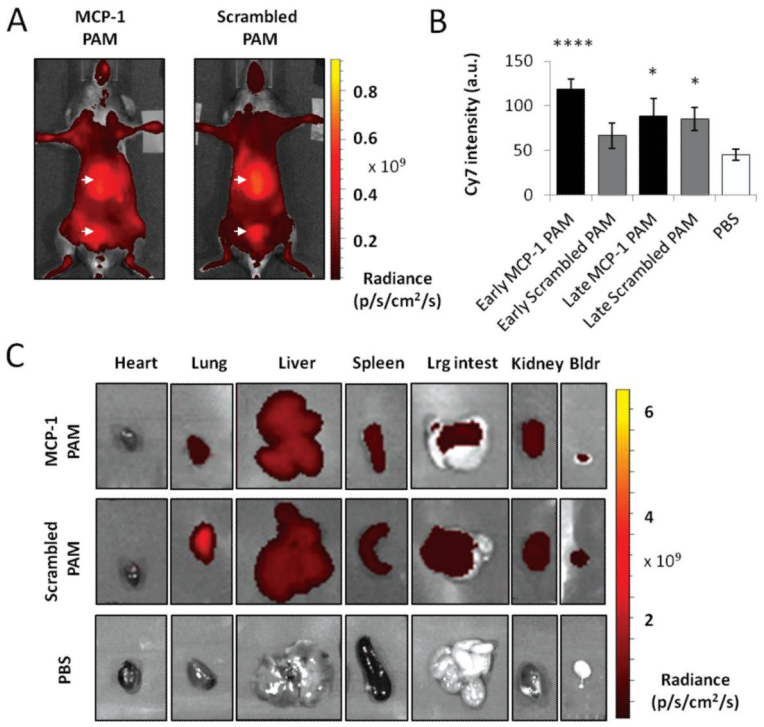

Figure 4.

Clearance and biodistribution of PAMs**.** Representative, whole body, in vivo optical images of ApoE knock-out mice treated with A) MCP-1 PAMs or scrambled PAMs. Arrows point to the liver and the bladder. B) Quantification of the Cy7 fluorescence signal in urine. Data points are mean ± SD, **P* < 0.05, ***P* < 0.01, ****P* < 0.001, ****P* < 0.0001 compared to the PBS-treated group. C) Ex vivo imaging of the heart, lung, liver, spleen, large intestines, kidney, and bladder treated with MCP-1 PAM, scrambled PAM, or PBS.

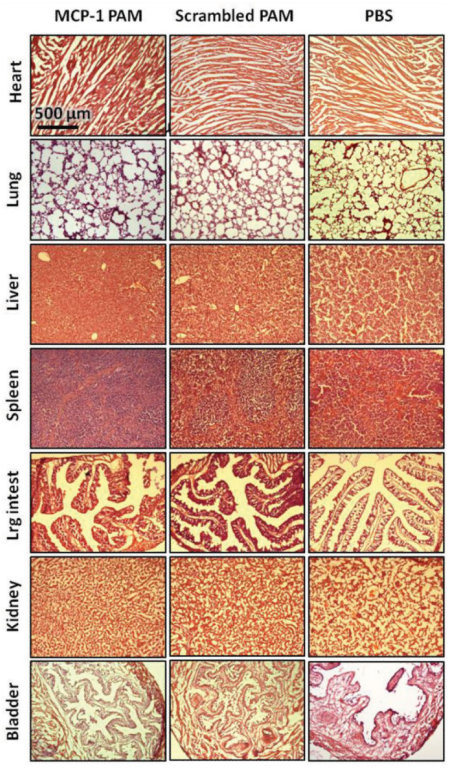

Figure 5.

Representative H and E staining of the organs upon PAM administration**.** No morphological changes or tissue damage was demonstrated in the heart, lung, liver, spleen, large intestines, kidney, and bladder treated with MCP-1 PAM or scrambled PAM, compared to PBS-treated controls.

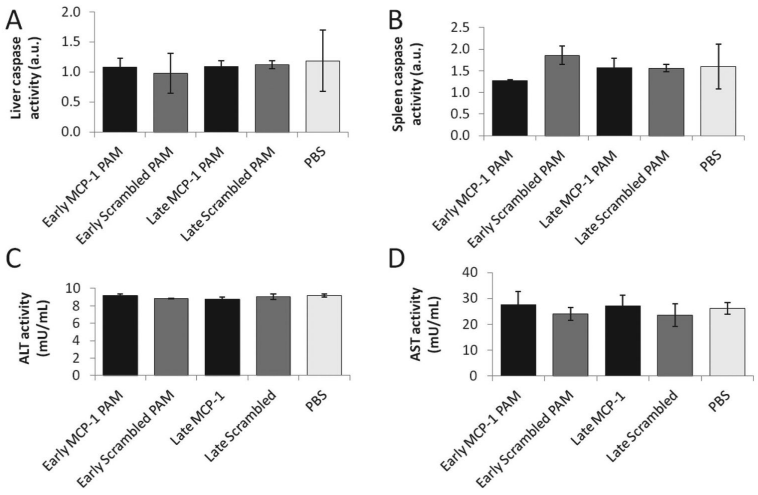

Figure 6.

Function of the liver and spleen upon PAM administration. A) Liver and B) spleen caspase activity of early- and late-stage ApoE knock-out mice treated with MCP-1 or scrambled PAMs show no statistical significance with early-stage mice treated with PBS. Liver function was assessed via C) alanine aminotransferase (ALT) and D) aspartate aminotransferase activity (AST). Data points are mean ± SD and no statistical significance was found for all assays when compared to early-stage mice treated with PBS.

Table 1

Materials characterization of PAMs.

	MCP-1 PAM	Scrambled PAM	MCP-1 peptide	Scrambled peptide
CMC [μm]	2.2	1.6	–	–
Size [nm]	14.7 ± 1.4	13.1 ± 1.4	–	–
Zeta potential [mV]	11.6 ± 0.1	10.9 ± 3.4	–	–
Secondary structure				
Beta sheet [%]	45.9 ± 1.0	60.9 ± 2.9	34.2 ± 3.5	37.5 ± 6.2
Random coil [%]	53.4 ± 1.6	38.8 ± 2.3	65.8 ± 3.5	62.5 ± 6.2
Alpha helix [%]	0.7 ± 0.7	0.3 ± 0.7	0.0 ± 0.0	0.0 ± 0.0